

# Fission decay of $^{282}\text{Cn}$ studied using cranking inertia

D. N. Poenaru<sup>1,2,\*</sup> and R. A. Gherghescu<sup>1,2</sup>

<sup>1</sup>*Horia Hulubei National Institute of Physics and Nuclear Engineering (IFIN-HH),  
P.O. Box MG-6, RO-077125 Bucharest-Magurele, Romania*

<sup>2</sup>*Frankfurt Institute for Advanced Studies (FIAS),  
Ruth-Moufang-Str. 1, 60438 Frankfurt am Main, Germany*

(Dated: )

Superheavy nuclei produced until now are decaying mainly by  $\alpha$  emission and spontaneous fission. Calculated  $\alpha$  decay half-lives are in agreement with experimental data within one order of magnitude. The discrepancy between theory and experiment can be as high as ten orders of magnitude for spontaneous fission. We analyze a way to improve the accuracy by using the action integral based on cranking inertia and a potential barrier computed by the macroscopic-microscopic method with a two-center shell model. Illustrations are given for  $^{282}\text{Cn}$  which has a measured fission half-life.

PACS numbers: 24.75.+i, 25.85.Ca, 21.10.Tg, 27.90.+b

## INTRODUCTION

The heaviest superheavy (SH) elements [1–3] with atomic numbers  $Z = 107 - 112$  are produced in cold fusion reactions [4, 5] between targets  $^{208}\text{Pb}$  or  $^{209}\text{Bi}$  and beams with mass numbers  $A > 50$ ; hot fusion reactions between actinide nuclei and  $^{48}\text{Ca}$  [6] are used for those with  $Z = 113 - 118$ . Attempts to study  $Z = 120$  are reported [2, 7, 8]. The main decay modes are either  $\alpha$  decay or spontaneous fission. Spontaneous fission, the dominating decay mode in the region around Rf, becomes a relatively weaker branch compared to  $\alpha$ -decay for the majority of recently discovered proton-rich nuclides. According to our calculations [9–11] it would be possible to see also cluster decay (CD) [12, 13] for heavier SHs with  $Z > 121$ , unlike for  $Z = 87 - 96$ , where CD is a rare phenomenon in a huge background of alpha particles. Up to now the produced SHs are neutrondeficient nuclei far from the line of  $\beta$ -stability. In the future it is expected to synthesize SHs closer to  $\beta$ -stability line [14].

For spontaneous fission calculations we refer to Hartree-Fock-Bogoliubov approach with finite-range and density-dependent Gogny force [15] and self-consistent symmetry-unrestricted nuclear density functional with Skyrme energy density functional and cranking inertia [16]. The closest value to the experimental one was obtained by using a dynamical approach [17, 18]. Simple relationships [19–21] have also been used.

Previously we have shown [22] that calculated  $\alpha$  decay half-lives are in agreement with experimental data within one order of magnitude, while the discrepancy between theory and experiment can be as high as ten orders of magnitude for spontaneous fission. It was clear that Werner-Wheeler approximation [23, 24] for the nuclear inertia leads to too small values to explain the measured spontaneous fission half-life. In the present work we try a better method based on the microscopic cranking inertia [25–27] introduced by Inglis [28]. Deformation energy and the inertia tensor are calculated in order to deter-

mine the half-life. Potential barrier is computed by the macroscopic-microscopic method [29] with a two-center shell model [30].

## DEFORMATION ENERGY

In a spontaneous fission process we obtain a light,  $^{A_2}\text{Z}_2$ , and a heavy,  $^{A_1}\text{Z}_1$ , fragment with radii  $R_2$  and  $R_1$  from a parent nucleus,  $^AZ$ , with a radius  $R_0$ :

$$^AZ \rightarrow ^{A_1}\text{Z}_1 + ^{A_2}\text{Z}_2 \quad (1)$$

According to the macroscopic-microscopic method the deformation energy of a nucleus,  $E_{def}$ , is calculated as a sum of two terms coming from a phenomenological (e.g. Yukawa-plus exponential model (Y+EM)),  $E_{macro} = E_{Y+EM}$ , and a small shell-plus-pairing correction,  $E_{micro} = \delta E$ :

$$E_{def} = E_{Y+EM} + \delta E \quad (2)$$

The shape-dependent terms in the LDM are the surface energy due to the strong interactions, tending to hold the nucleons together, and the electrostatic (Coulomb) energy, acting in the opposite direction. By requesting zero deformation energy for a spherical shape,

$$E_{Y+EM} = (E_Y - E_Y^0) + (E_c - E_c^0) \quad (3)$$

the Coulomb energy and the nuclear energy are both expressed as double-volume integrals:

$$E_Y = -\frac{a_2}{8\pi^2 r_0^2 a^4} \int_{V_n} \int \left( \frac{r_{12}}{a} - 2 \right) \frac{\exp(-r_{12}/a)}{r_{12}/a} d^3 r_1 d^3 r_2 \quad (4)$$

where  $r_{12} = |\mathbf{r}_1 - \mathbf{r}_2|$ ,  $a$  is the diffusivity parameter, and  $a_2 = a_s(1 - \kappa I^2)$ ,  $I = (N - Z)/A$ .

$$E_c = \frac{1}{2} \int_{V_n} \int \frac{\rho_e(\mathbf{r}) \rho_e(\mathbf{r}_1) d^3 r d^3 r_1}{|\mathbf{r} - \mathbf{r}_1|} \quad (5)$$

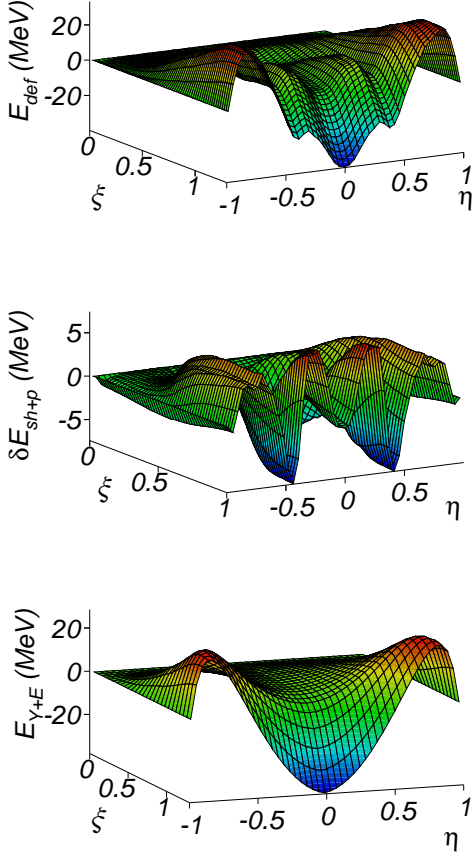


FIG. 1. (Color online) PES of  $^{282}\text{Cn}$  vs  $\xi$  and  $\eta$ . Y+EM (bottom), shell + pairing corrections (center), and total deformation energy (top). The deepest two valleys in the central figure are due to the magicity of the daughter  $^{208}\text{Pb}$  for  $^{74}\text{Zn}$  radioactivity at about  $\eta = 0.47$  and of the light fragment  $^{132}\text{Sn}$  at  $\eta \simeq 0$ .

with  $\rho_e$  the charge density.

Potential energy surfaces [31] are calculated by using the most advanced asymmetric two-center shell model allowing to obtain shell and pairing corrections which are added to the Yukawa-plus-exponential model deformation energy [32] taking into account the difference between charge and mass asymmetry [33]. The model parameters are taken from Möller et al. [34].

Starting from the touching point configuration,  $R \geq R_t = R_1 + R_2$ , for spherical shapes of the fragments, one can use *analytical relationships*. The Coulomb interaction energy of a system of two spherical nuclei, separated by a distance  $R$  between centers, is  $E_{c12} = e^2 Z_1 Z_2 / R$ , where  $e$  is the electron charge.

Within a liquid drop model (LDM) there is no contribution of the surface energy to the interaction of the separated fragments; the barrier has a maximum at the touching point configuration. The proximity forces acting at small separation distances (within the range of

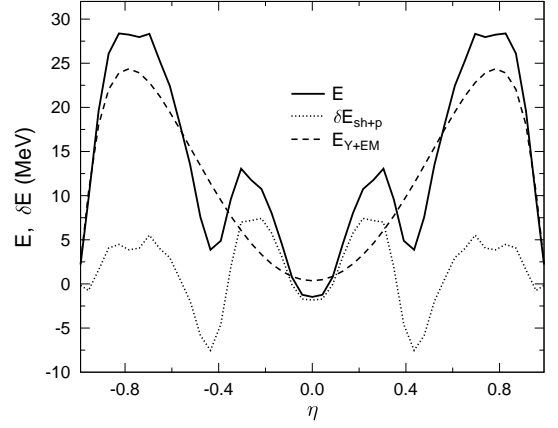


FIG. 2. (Color online) Deformation energies at the touching point configurations ( $R = R_t$ ) of  $^{282}\text{Cn}$  vs the asymmetry  $\eta$ : macroscopic energy  $E_{Y+EM}$ ; shell + pairing corrections  $\delta E_{sh+p}$  and their sum  $E = E_{def}$ .

strong interactions) give rise in the Y+EM to an interaction term expressed as follows

$$E_{Y12} = -4 \left( \frac{a}{r_0} \right)^2 \sqrt{a_{21} a_{22}} \frac{\exp(-R/a)}{R/a} \cdot [g_1 g_2 (4 + \frac{R}{a}) - g_2 f_1 - g_1 f_2] \quad (6)$$

where

$$g_k = \frac{R_k}{a} \cosh \left( \frac{R_k}{a} \right) - \sinh \left( \frac{R_k}{a} \right) \quad (7)$$

$$f_k = \left( \frac{R_k}{a} \right)^2 \sinh \left( \frac{R_k}{a} \right) \quad (8)$$

In order to obtain a relatively smooth potential energy surface (PES) we made the approximation for mass and charge asymmetry  $\eta = \eta_A = (A_1 - A_2)/A \simeq \eta_Z = (Z_1 - Z_2)/Z$ . We prefer to use the dimensionless separation distance  $\xi = (R - R_i)/(R_t - R_i)$  instead of  $R$ . Here  $R_i = R_0 - R_2$ . In this way one can clearly see the touching point configuration at  $\xi = 1$ . We also adopt the usual convention of having zero deformation energy and shell plus pairing corrections for the initial spherical shape, leading to  $E_{def} = E_{Y+EM} = \delta E = 0$  at  $R = R_i$  for all values of  $\eta$  and at  $\eta = \pm 1$  for all values of  $R$ .

The PES of  $^{282}\text{Cn}$  versus the normalized separation distance  $\xi$  and the mass asymmetry  $\eta$  are plotted in Fig. 1. The macroscopic Y+EM deformation energy is shown at the bottom, followed by the microscopic shell plus pairing corrections (center), and their sum (the total deformation energy) at the top. Two valleys around  $|\eta| \simeq 0$  and  $0.47$  can be seen in the center of Fig. 1 as well as in Fig. 2 at the touching point  $R = R_t$ . They are produced due to the magicity of the nucleon number of one of the fragments around  $^{132}\text{Sn}$  and  $^{208}\text{Pb}$ , respectively.

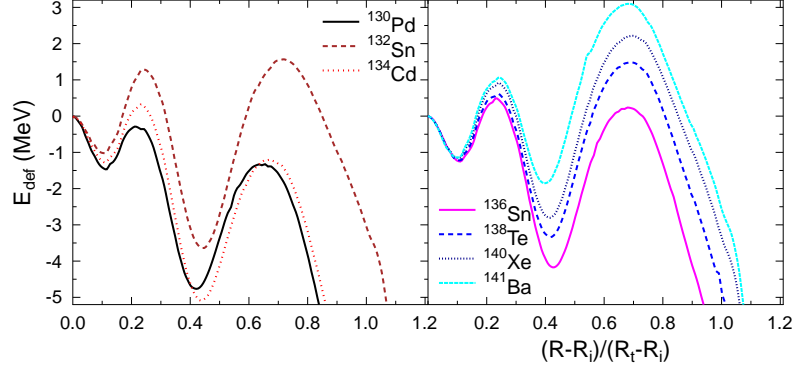


FIG. 3. (Color online) Potential barriers for the spontaneous fission of  $^{284}\text{Cn}$  with light fragments  $^{130}\text{Pd}$ ,  $^{132}\text{Sn}$ ,  $^{134}\text{Cd}$  (left) and  $^{136}\text{Sn}$ ,  $^{138}\text{Te}$ ,  $^{140}\text{Xe}$ ,  $^{141}\text{Ba}$  (right).

Every time a nucleon number reaches a magic value, the corresponding shell correction has a local minimum.

Few fission channels could be efficiently used to test the method of calculating spontaneous fission half-lives of  $^{282}\text{Cn}$  whose experimental value is known. We know from the mass distributions of fission fragments that few splittings give the largest yield, very likely explained by shell effects (spherical and/or deformed magic numbers of neutrons and protons). Consequently we can guess that the channels having the light fragments shown in Fig. 3 would be among those major splittings.

### NUCLEAR INERTIA AND THE HALF-LIFE

After including the BCS pairing correlations [35], the components of the inertia tensor is given by [36]:

$$B_{ij} = 2\hbar^2 \sum_{\nu\mu} \frac{\langle \nu | \partial H / \partial \beta_i | \mu \rangle \langle \mu | \partial H / \partial \beta_j | \nu \rangle}{(E_\nu + E_\mu)^3} (u_\nu v_\mu + u_\mu v_\nu)^2 \quad (9)$$

where  $H$  is the single-particle Hamiltonian allowing to determine the energy levels and the wave functions  $|\nu\rangle$ ;  $u_\nu$ ,  $v_\nu$  are the BCS occupation probabilities,  $E_\nu$  is the quasiparticle energy. Other involved quantities are the pairing gap  $\Delta$  and the Fermi energy  $\lambda$  [37]. The multidimensional hyperspace of deformation parameters is defined by  $\beta_1, \beta_2, \dots, \beta_n$ . The dimension of any component,  $B_{ij}$ , of the tensor is a mass. By choosing the distance between fragments,  $R$ , as deformation coordinate, the effective mass at the touching point of the two fragments should be equal to the reduced mass  $\mu = (A_1 A_2 / A) m$ , where  $m$  is the nucleon mass. Sometime the inertia tensor is called a mass tensor. Similar to the shell correction energy, the total inertia is the sum of contributions given by protons and neutrons  $B_{ij} = B_{ij}^p + B_{ij}^n$ .

The kinetic energy

$$E_k = \frac{1}{2} \sum_{i,j=1}^n B_{ij}(\beta) \frac{d\beta_i}{dt} \frac{d\beta_j}{dt} \quad (10)$$

includes the change in time of the nuclear shape (the time derivatives).

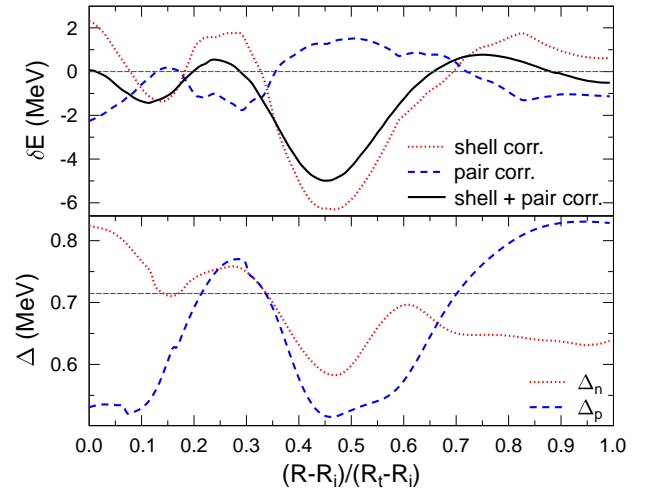


FIG. 4. (Color online) Shell and pairing corrections (top), pairing gap (bottom) versus  $(R - R_i)/(R_t - R_i)$  for the fission of  $^{282}\text{Cn}$  into  $^{130}\text{Pd} + ^{152}\text{Dy}$  fragments. Proton and neutron component are shown.

By choosing four independent deformation parameters  $R, b_2, \chi_1, \chi_2$  [24] during the deformation from one parent nucleus to two fission fragments, the surface equation in cylindrical coordinates  $\rho, z$  is given by:

$$\rho_s^2(z; b_1, \chi_1, b_2, \chi_2) = \begin{cases} b_1^2 - \chi_1^2 z^2 & , -a_1 < z < z_c \\ b_2^2 - \chi_2^2 (z - R)^2 & , z_c < z < R + a_2 \end{cases} \quad (11)$$

where  $z_c$  is the position of the crossing plane. The semi-axes ratio of spheroidally deformed fragments are denoted by  $\chi_1 = b_1/a_1$ ,  $\chi_2 = b_2/a_2$ . The scalar,  $B(R)$ , is determined by the components of the tensor and the partial derivatives with respect to  $R$ :

$$B(R) = B_{b_2 b_2} \left( \frac{db_2}{dR} \right)^2 + 2B_{b_2 \chi_1} \frac{db_2}{dR} \frac{d\chi_1}{dR} + 2B_{b_2 \chi_2} \frac{db_2}{dR} \frac{d\chi_2}{dR} + 2B_{b_2 R} \frac{db_2}{dR} + B_{\chi_1 \chi_1} \left( \frac{d\chi_1}{dR} \right)^2 + 2B_{\chi_1 \chi_2} \frac{d\chi_1}{dR} \frac{d\chi_2}{dR} + 2B_{\chi_1 R} \frac{d\chi_1}{dR} + B_{\chi_2 \chi_2} \left( \frac{d\chi_2}{dR} \right)^2 + 2B_{\chi_2 R} \frac{d\chi_2}{dR} + B_{RR} \quad (12)$$

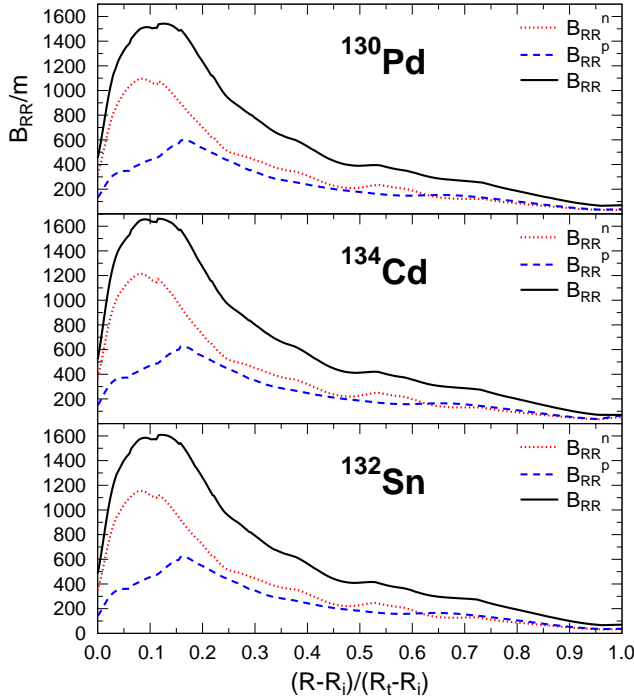


FIG. 5. (Color online) The component  $B_{RR}/m$  of the inertia tensor versus  $(R - R_i)/(R_t - R_i)$  for the fission of  $^{282}\text{Cn}$  with light fragments  $^{130}\text{Pd}$ ,  $^{134}\text{Cd}$ , and  $^{132}\text{Sn}$ . Proton and neutron components are shown.

One of the most important binary split of  $^{282}\text{Cn}$  leads to  $^{130}\text{Pd} + ^{152}\text{Dy}$  fragments. As it is shown in Fig. 4, the variation of the shell plus pairing correction (top) determines the pairing gaps,  $\Delta_n$  and  $\Delta_p$  (bottom), as solutions of the BCS system of two eqs. also allowing to find the Fermi energies  $\lambda_n$  and  $\lambda_p$  [37, 38]. Their influence on the inertia components  $B_{RR}^n/m$  and  $B_{RR}^p/m$  is also clear from the Figure 5.  $B_{RR}$  is the most important component of the inertia tensor if we consider spherical shapes and keep constant the radius  $R_2$  of the light fragment. When we compare  $B_{RR}/m$  for the binary fission  $^{282}\text{Cn} \rightarrow ^{130}\text{Pd} + ^{152}\text{Dy}$  (see the top of Fig. 5) with those corresponding to  $^{282}\text{Cn} \rightarrow ^{134}\text{Cd} + ^{148}\text{Gd}$  (center of Fig. 5) and to that of  $^{282}\text{Cn}$  fission with light fragment  $^{132}\text{Sn}$  (bottom of Fig. 5) it is clear that the first one is smaller than the two others. Having also in mind a broader potential barrier we may expect a longer half-life for this split. The three curves are very similar as it should be due to the fact that the shell plus pairing effects are not very much different for these neighbouring light fragments ( $Z_2, N_2$  (46, 84) for  $^{130}\text{Pd}$ , (50, 82) for  $^{132}\text{Sn}$ , and (48, 86) for  $^{134}\text{Cd}$ ). In all three cases neutron contribution is larger than the proton one. Intuitively we can guess that an exponential approximation would be appropriate in the interval of the variable  $\xi$  between the two turning points.

The half-life of a parent nucleus  $AZ$  against the split into a light fragment  $A_2Z_2$  and a heavy fragment  $A_1Z_1$  is given by

$$T = [(\hbar \ln 2)/(2E_v)] \exp(K_{ov} + K_s) \quad (13)$$

and is calculated by using the Wentzel–Kramers–Brillouin (WKB) quasiclassical approximation, according to which the

action integral is expressed as

$$K = \frac{2\sqrt{2m}}{\hbar} \int_{R_a}^{R_b} \{[(B(R)/m)][E_{def}(R) - E_{def}(R_a)]\}^{1/2} dR \quad (14)$$

with  $B$  = the cranking inertia,  $K = K_{ov} + K_s$ , and the  $E(R)$  potential energy of deformation.  $R_a$  and  $R_b$  are the turning points of the WKB integral where  $E_{def} = E_{def}(R_a) = E_{def}(R_b)$ . The two terms of the action integral  $K$ , correspond to the overlapping ( $K_{ov}$ ) and separated ( $K_s$ ) fragments. We can use the relationship

$$\log_{10} T = 0.43429(0.4392158S_{ab}) - 20.8436 - \log_{10} E_v \quad (15)$$

where

$$S_{ab} = \int_{R_a}^{R_b} \{[(B(R)/m)][E_{def}(R) - E_{def}(R_a)]\}^{1/2} dR \quad (16)$$

TABLE I. Decimal logarithm of fission half-lives  $\log_{10} T_f(s)$  of  $^{282}\text{Cn}$  with different light fragments and zero point vibration energies. Experimental value:  $\log_{10} T_f^{exp}(s) = -3.086$

Light fragment	$E_v$ (MeV)	$\log_{10} T_f(s)$
$^{130}\text{Pd}$	0.50000	-3.4278
	0.43680	-3.0860
$^{134}\text{Cd}$	0.50000	-2.4881
	0.60289	-3.0860
$^{132}\text{Sn}$	0.50000	5.5076
	1.96620	-3.0860

The computer programme developed by one of us (RAG) to calculate the half-life starts by making a search for the largest barrier height near the deepest minimum (the ground-state). The two turning points are found in the next step. Usually for superheavy nuclei the second turning point corresponds to separated fragments inside,  $R_b < R_t$ , or outside,  $R_b > R_t$ , the touching point.

In Table I we present the results of our calculations concerning the half-life for spontaneous fission of  $^{282}\text{Cn}$ . It is clear that an important binary split will produce the light fragment  $^{130}\text{Pd}$  — the same giving the thinnest (most penetrable) potential barrier in Fig. 3. On the other hand when the light fragment is  $^{134}\text{Cd}$  or  $^{132}\text{Sn}$  the half-life is longer for the same zero-point vibration energy. We can conclude that by using the cranking inertia it is possible to reproduce the spontaneous fission half-life with a reasonable value of the zero-point vibration energy.

This work is partially supported within the IDEI Programme under contracts 43/05.10.2011 and 42/05.10.2011 with UEFISCDI, and NUCLEU Programme, Bucharest.

\* poenaru@fias.uni-frankfurt.de

[1] J. H. Hamilton, S. Hofmann, and Y. Oganessian, Ann. Rev. Nucl. Part. Sci. **63**, 383 (2013).

- [2] J. Khuyagbaatar *et al.*, Phys. Rev. Lett. **112**, 172501 (2014).
- [3] A. Sobiczewski, Radiochimica Acta **99**, 395 (2011).
- [4] S. Hofmann and G. Münzenberg, Rev. Mod. Phys. **72**, 733 (2000).
- [5] K. Morita *et al.*, J. Phys. Soc. Jpn. **76**, 045001 (2007).
- [6] Y. T. Oganessian, J. Phys. G: Nucl. Part. Phys. **34**, R165 (2007).
- [7] Y. T. Oganessian *et al.*, Phys. Rev. C **79**, 024603 (2009).
- [8] S. Hofmann, 2011, private communication.
- [9] D. N. Poenaru, R. A. Gherghescu, and W. Greiner, Phys. Rev. Lett. **107**, 062503 (2011).
- [10] D. N. Poenaru, R. A. Gherghescu, and W. Greiner, Phys. Rev. C **85**, 034615 (2012).
- [11] D. N. Poenaru, R. A. Gherghescu, and W. Greiner, J. Phys. G: Nucl. Part. Phys. **39**, 015105 (2012).
- [12] Encyclopaedia Britannica online, <http://www.britannica.com/EBchecked/topic/465998/>.
- [13] A. Sandulescu, D. N. Poenaru, and W. Greiner, Sov. J. Part. Nucl. **11**, 528 (1980).
- [14] V. I. Zagrebaev and W. Greiner, Phys. Rev. C **87**, 034608 (2013).
- [15] M. Warda and J. L. Egido, Phys. Rev. C **86**, 014322 (2012).
- [16] A. Staszczak, A. Baran, and W. Nazarewicz, Phys. Rev. C **87**, (2013).
- [17] R. Smolanczuk, Phys. Rev. C **56**, 812 (1997).
- [18] R. Smolanczuk, J. Skalski, and A. Sobiczewski, Phys. Rev. C **52**, 1871 (1995).
- [19] X. Bao, H. Zhang, G. Royer, and J. Li, Nucl. Phys. A **906**, 1 (2013).
- [20] K. P. Santhosh, R. K. Biju, and S. Sahadevan, Nucl. Phys. A **832**, 220 (2010).
- [21] C. Xu, Z. Ren, and Y. Guo, Phys. Rev. C **78**, 044329 (2008).
- [22] D. N. Poenaru, R. A. Gherghescu, and W. Greiner, J. Phys. G: Nucl. Part. Phys. **40**, 105105 (2013).
- [23] R. A. Gherghescu, W. Greiner, and D. N. Poenaru, Phys. Rev. C **52**, 2636 (1995).
- [24] R. A. Gherghescu and D. N. Poenaru, Phys. Rev. C **72**, 027602 (2005).
- [25] R. A. Gherghescu and D. N. Poenaru, E-print Cite as: arXiv:1106.xxxxv1 [nucl-th], IFIN-HH, (unpublished), at <http://arXiv.org/> Cornell University.
- [26] W. Schneider, J. A. Maruhn, and W. Greiner, Z. Phys. A **323**, 111 (1986).
- [27] D. N. Poenaru, R. A. Gherghescu, and W. Greiner, Europ. Phys. J. A **24**, 355 (2005).
- [28] D. R. Inglis, Phys. Rev. **96**, 1059 (1954).
- [29] V. M. Strutinsky, Nucl. Phys. A **95**, 420 (1967).
- [30] R. A. Gherghescu, Phys. Rev. C **67**, 014309 (2003).
- [31] D. N. Poenaru, R. A. Gherghescu, and W. Greiner, Phys. Rev. C **73**, 014608 (2006).
- [32] H. J. Krappe, J. R. Nix, and A. J. Sierk, Phys. Rev. C **20**, 992 (1979).
- [33] D. N. Poenaru, M. Ivaşcu, and D. Mazilu, Comp. Phys. Commun. **19**, 205 (1980).
- [34] P. Möller, J. R. Nix, W. D. Myers, and W. J. Swiatecki, Atomic Data Nucl. Data Tables **59**, 185 (1995).
- [35] J. Bardeen, L. Cooper, and J. Schrieffer, Phys. Rev. C **108**, 1175 (1957).
- [36] M. Brack *et al.*, Rev. Mod. Phys. **44**, 320 (1972).
- [37] D. N. Poenaru, R. A. Gherghescu, C. Anghel, and W. Greiner, Rom. Rep. Phys. **64**, **Supplement**, 1329 (2012).
- [38] D. N. Poenaru and I. H. Plonski, in *Nuclear Decay Modes*, Ed. D. N. Poenaru (Institute of Physics Publishing, Bristol, 1996), Chap. 11, pp. 433–486.